

## Seismic moment tensor and dynamic parameters of earthquakes in the Central Tien Shan

© 2020 Nailia A. Sycheva

Research Station of the Russian Academy of Sciences in Bishkek City, Bishkek, Kyrgyzstan  
E-mail: [nelya@gdirc.ru](mailto:nelya@gdirc.ru)

**Abstract.** In the study, seismic moment tensors (SMT) of 177 earthquakes in the Central Tien Shan with  $K \geq 10.5$  ( $M \geq 3.6$ ) occurring from 2007 to 2017 are determined on the basis of the wave inversion method and data from the KNET seismic network. The 177 obtained solutions have been added to an SMT catalogue, which includes 284 events with  $2.8 \leq M \leq 6$  that have occurred from 1996 to 2017. Some characteristics of the SMT catalogue are discussed along with constructed principal stress axes azimuth diagrams and dip angle distribution graphs. For the most part of events, the compression axis of the seismic events has a north-northwest direction and a subhorizontal orientation; the direction of the tension axis does not have a pronounced maximum, while for most events it has a subvertical orientation. In addition to the scalar seismic moment, the dynamic parameters (DP) of the 150 events from the SMT catalogue that have occurred from 1999 to 2014 were computed: the source radius (Brune radius) and tangential stress drop. Studied correlations between the DP and magnitude show the link between the stress drop and earthquake magnitude to be the weakest. The Lode–Nadai factor distribution on the grounds of the seismic moment tensors from the SMT catalogue was constructed and the deformation types typical for the studied area were identified. A comparison between deformation regimes and stress drop values is presented.

**Keywords:** earthquake, seismic moment tensor, scalar seismic moment, moment magnitude, corner frequency, source radius, stress drop, Lode–Nadai factor.

**For citation:** Sycheva N.A. Seismic moment tensor and dynamic parameters of earthquakes in the Central Tien Shan. *Geosistemy perekhodnykh zon = Geosystems of Transition Zones*, 2020, vol. 4, no. 2, pp. 192–209. (In Engl.). <https://doi.org/10.30730/gtrz.2020.4.2.178-191.192-209>.

### Introduction

The Central Tien Shan extends over the wide territory, bounded with the Fergana Range in the west, Zailiysk, Kyrgyz and Talas Alatau ranges in the north, Meridional Range in the east and Kokshaal-Too Range in the south (<https://silkadv.com/ru/node/410>). It is customary to refer the Zailiysk Alatau, Kungey Alatau, Ketmen and Kyrgyz Alatau (the Kyrgyz Range) to the Northern Tien Shan (<http://tianshan.alnaz.ru/objekty/hrebty.html>). The Kyrgyz Range

bounds the Central Tien Shan from the north, belonging thereby to both regions at once. KNET the seismic network, organized on the Northern Tien Shan in 1991, includes 10 digital wideband stations. The major part of the stations is located in northern foothills of the Kyrgyz Range and along the rims of the Chuy Depression. Despite the fact that the KNET network stations are located on the Northern Tien Shan territory, they allow to register the earthquakes occurring in the Central Tien Shan.

Translation of the article published in the present issue of the Journal: Сычева Н.А. Тензор сейсмического момента и динамические параметры землетрясений Центрального Тянь-Шаня. *Translation by G.S. Kachesova.*

Based on the data of the KNET network the earthquakes catalogues are formed, focal mechanisms and dynamic parameters of earthquakes are determined, and other scientific problems are also solved. The data on focal mechanisms of earthquakes are used for estimation of stress-strain state of the medium. Earthquakes dynamic parameters, the stress drop among them, can also characterize the regional peculiarities of the crust straining process. These data accumulation allows to estimate the geodynamics processes, proceeding within the medium.

Two approaches are used for the focal mechanisms of the sources: mechanism determination by the sign of the *P*-wave arrival [Reasenberg, Oppenheimer, 1985; Snoke, 1989, 1990, 2000; et al.] and the waveform inversion method [Dziewonski et al., 1981; Fukahata et al., 2003; Kostiuk et al., 2010; et al.].

One of the conditions of reliable focal mechanism determination by the signs of the *P*-waves arrival is a total surrounding of the epicenter with observation stations. The configuration of the KNET network stations is able to reveal source mechanisms by this method only for those earthquakes, that have occurred in the territory, bounded with the coordinates of the network marginal stations: 42.0–43.0° N and 73.75–76.0° E, that represents a small area of 100 × 300 km<sup>2</sup> (fig. 1). The waveform inversion method allows to calculate the seismic moment tensors on the base of the KNET network data and, consequently, to determine the focal mechanism also for the earthquakes occurred in the territory outside the stations location within 1–2° (see the fig. 1). In present work we refer this territory to the Central Tien Shan.

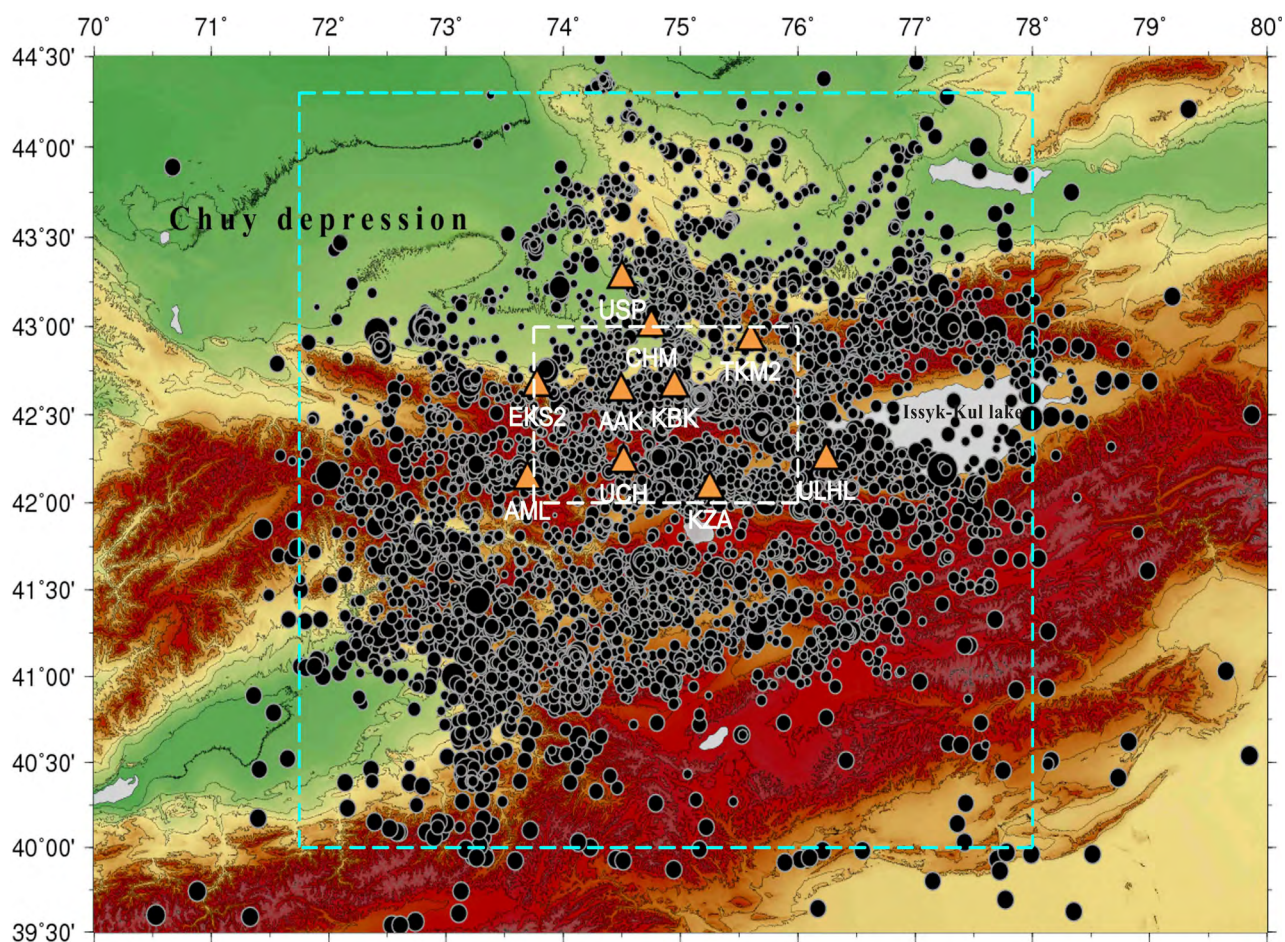


**Figure 1.** Location of the earthquakes epicenters from the catalogue according to the KNET network (more than 9000 events, 1994–2017). Triangles – the KNET network stations. The white dashed line conventionally indicates the territory, bounded with the coordinates of the marginal stations of the KNET network. For the earthquakes in this area, focal mechanisms are determined by the signs of the *P*-waves arrival. The turquoise dashed line conventionally indicates the territory for which the waveform inversion method is applied.

The waveform inversion method for SMT computation is used at the Research Station of the RAS since 2006. On its basis the seismic moments tensors of 107 earthquakes for 1996–2006 have been determined [Kostiuk, 2008; Kostiuk et al., 2010]. The solutions obtained in [Kostiuk, 2008] are noted to conform well with those represented in the catalog of CMT (Centroid moment tensors) (<https://www.globalcmt.org/CMTsearch.html>) for the earthquakes with  $M > 4.5$  ( $K > 12$ ).

The source radiation directivity is very important when the source spectrum constructing, on which base the earthquakes dynamic parameters are calculated. Therefore, only those events were considered in the works [Sycheva, Bogomolov, 2014, 2016] when the source studying, which had been occurred in the territory, that was not beyond the KNET network boundaries.

The present work task is to determine the seismic moment tensors for the earthquakes, occurred in 2007–2017 in the territory of location of the KNET network stations and outside its boundaries within  $1-2^\circ$ , and to update the SMT catalogue by this means. Basic characteristics of the obtained catalogue are given in the article.

Availability of values of the  $f_0$  corner frequency for the earthquakes of 1999–2014, occurred in the Central Tien Shan territory [Sychev et al., 2018], have allowed to solve the second task – to calculate the dynamic parameters (the source radius and tangential stress drop) for the earthquakes with  $M = 2.8-6$  from the SMT catalog, expanding in this way the database, and, respectively, the territory, for which they have been determined. Further, obtained data can be used for estimation of some parameters of stress-strain state of the studied territory.

### Initial data and methodologies

#### *Methodology of seismic moment tensor computation*

To calculate the SMT, we took the earthquakes of 2007–2017 occurred in the KNET network stations location and outside it at

a distance of  $1-2^\circ$  in a radius with the energy class  $K \geq 10.5$  ( $M > 3.5$ ). We also considered several earthquakes below this class, for which the SMT determination became possible. The SMT computation for the events of 2007–2010 was carried out on the base of waveforms, obtained in miniSEED format with a frequency of 40 Hz from the website of the IRIS Consortium (Incorporated Research Institutions for Seismology) (<https://ds.iris.edu/ds/nodes/dmc/data/types>). And the records with a frequency of 100 Hz from the archive of the Research Station of the RAS were used for the events of 2011–2017. The earthquakes records were previously converted from the S4 (SEED) to the miniSEED format with the authoring software [Sychev, Sycheva, 2018]. Determination of the  $P$ -wave arrival time was carried out with the SAC (Seismic Analysis Code) software (<http://ds.iris.edu/files/sac-manual>) over all components ( $E$ ,  $N$ ,  $Z$ ).

Seismic moment tensors for studied earthquakes have been determined with the software, developed by Yu. Yagi [Yagi, 2004], which realizes the waveform inversion method. In this software the Green's function is calculated by the Kohketsu method [Kohketsu, 1985], modified in [Kikuchi, Kanamori, 1991], at that the inversion procedure is constructed in accordance with [Fukahata et al., 2003].

When the Green's function calculating for the studied territory, the velocity model of the Institute of geosphere dynamics of the RAS [Zemnaia... , 2006] have been used, rocks densities are specified according to [Kurskeev et al., 2004], the attenuation have been determined on the base of the geological map [Geologicheskaia... , 1980] and from the tables of rock properties [Lay, Wallace, 1995]. The waveform inversion method is described in detail in the works [Yagi, 2004; Kostiuk, 2008; Kostiuk et al., 2010].

The program for the seismic moment tensors computation outputs graphic files, which examples are presented in the figure 2. The first example (fig. 2 a) demonstrates the solution, obtained from 18 records of the earthquake (9 stations),

the second – on the base of 13 records (6 stations) (fig. 2 b). In the both cases we have a good result of the modelling: the value of discrepancy (variance) is equal 0.08. This indicates that an acceptable solution may be obtained even with few analyzed seismograms. The focal mechanisms presented in the figure 2 have a thrust type, and the compression axis azimuth has a submeridian direction, that corresponds to the regional geodynamic regime. Output graphic file contains not only the graphic image of a focal mechanism, but the assessments of the earthquake focal parameters. These pa-

rameters are as follows: the angles describing the nodal planes position (strike, dip, slip), the deformation tensor components, as well as the  $M_0$  scalar seismic moment (determined when the inversion method using) and the moment magnitude  $M_w$  (see the fig. 2). Then, the values of the nodes of nodal planes are used to determine the parameters of the principal stress axes – the azimuth and the dip angle – with the sdrtpb.m program from the SEIZMO Suite (Passive seismology toolbox for Matlab & GNU Octave) (<http://epsc.wustl.edu/~ggeuler/codes/m/seizmo>).

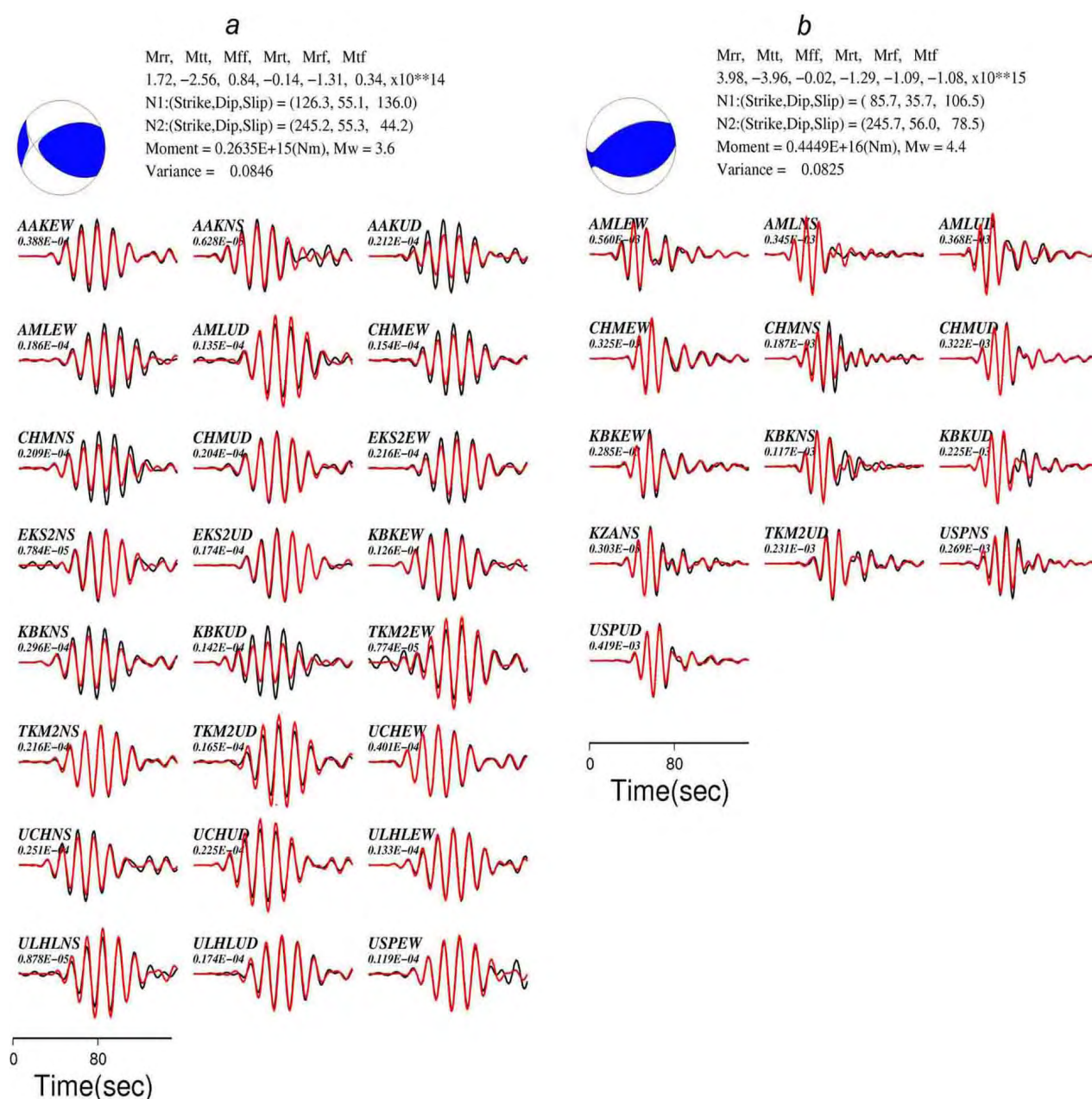


**Figure 2.** Example of graphic output file of the seismic moment tensor computation for two earthquakes: (a) 2017.07.29,  $K = 11.7$ ; (b) 1998.11.21,  $K = 12.5$ . Red lines – synthetic seismograms, black – initial seismograms.

### *Methodology of the dynamic parameters computation*

The source radius is determined with the formula [Scholz, 2019; Abercrombie, Rice, 2005; Scuderi et al., 2016]:

$$r = kV_s / f_0, \quad (1)$$

where  $f_0$  – corner frequency (inverse fracture time in a source),  $V_s$  –  $S$ -wave speed,  $k$  – numerical factor dependent on the model of rupture in a source. We use the Brune model in our case. The expression (1) determines the so-called Brune radius for this model [Brune, 1970],  $k = 0.37$ . The simplest Brune model supposes the slip to occur simultaneously and «instantly» over all the fault plane, that has a circle form with the  $r$  radius. The form of a source is spherical with the same radius.

General correlation between the stress drop, the seismic moment and the geometrical parameters of a source [Ruff, 1999; Madariaga, 1979; Kocharian, 2016]:

$$\Delta\sigma = C_\sigma M_0 / S_{r_1} \approx C_\sigma M_0 / S^{3/2}. \quad (2)$$

The expression for the stress drop (2) may be simplified for the case of the circular fault plane with a radius  $r$ , and the square  $S = \pi r^2$ . It is radius  $r$  that may be accepted as a typical size of a source,  $r_1$ , and the simplified expression for  $\Delta\sigma$  takes the form  $\Delta\sigma = C_\sigma M_0 / \pi r^3$ . The value of the  $C_\sigma$  factor for this case is determined in the work [Eshelby, 1957]:  $C_\sigma = 7\pi/16 \approx 1.37$ , and we get from (2) the following expression:

$$\Delta\sigma = 7M_0 / 16r^3, \quad (3)$$

which is most often used to estimate the  $\Delta\sigma$  value by seismic data [Brune, 1970, 1971; Scholz, 2019].

One need the data on the corner frequency  $f_0$  and the  $S$ -wave speed to calculate the source radius (1), as well as the scalar seismic moment  $M_0$  and the source radius  $r$  – to determine the stress drop from (3).

The values of the  $f_0$  (determined by the  $S$ -wave) were taken from the work [Sychev et al., 2018], the  $S$ -wave speed was assumed to be

3.5 km/s [Roecker et al., 1993], and the values of the scalar seismic moment were taken from the SMT catalog. It is worth noting, that the waveforms of local earthquakes with a record frequency of 100 Hz were considered to build  $P$ - and  $S$ -waves spectra and to find the corner frequency  $f_0$  in the work [Sychev et al., 2018].

## **Results**

### *Characteristics of the SMT catalog*

The seismic moment tensors of 177 events have been determined as a result of the inversion method applying to digital records of local earthquakes of 2007–2017. It is already noted, that 107 SMT solutions for the earthquakes of 1996–2006 have been obtained in the works [Kostiuk, 2008; Kostiuk et al., 2010]. The final full catalogue includes 284 events. For each earthquake the catalogue contains date, time, epicenter, depth and energy characteristic ( $K$ ), parameters, describing the rupture kinematics in a source: angles, which characterize the nodal planes position (equiprobable fault planes), deformation tensor components, as well as azimuth and dip angle of the stress principal axis. The scalar seismic moment is assumed to be a dynamic (focal) characteristic and is considered as a measure of potential energy necessary to move the masses over the fault surface [Puzyrev, 1997].

Some statistical characteristics of the full catalogue are presented in the figure 3. The events with a magnitude  $M = 3.5$ –4 prevail in the catalogue. Their major part is occurred at the depth down to 20 km. The temporal distribution of the events is nonuniform. Maximal number seismograms used for solving is 30 (by 3 components –  $E$ ,  $N$ ,  $Z$  at 10 stations), but most of the solutions have been obtained when analyzed seismograms quantity is more than 5, but less than 15 (fig. 3 d).

The distribution of the value of discrepancy of wave modelling (variance) in initial and sorted form is presented in the figure 3 e, f. Minimal error amounts 0.03, and maximal – 0.4. For 120 events the modelling error does not exceed the value of 0.1, for 140 events – 0.2,

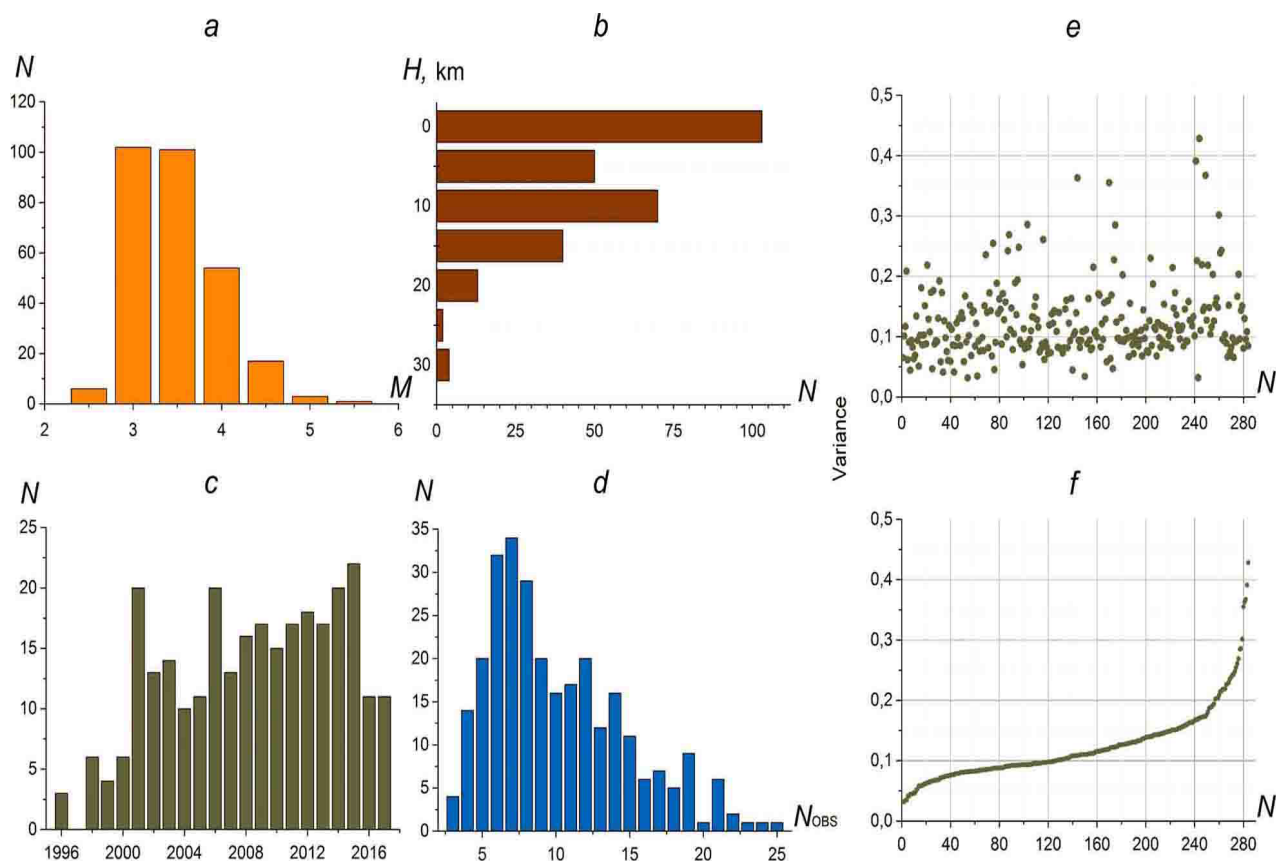


**Figure 3.** Histograms of events distribution in the SMT catalogue: a – by magnitude; b – by depth; c – by time; d – by the number of analyzed seismograms. Distribution of variance values of wave modeling for events in the seismic moment tensors catalogue: e – initial values; f – sorted values.

and only for 20 events (7 % from the total) it is in the range of 0.2–0.4 (significant error).

### Focal mechanisms

Epicenters of the earthquakes from the SMT (284 events) and their focal mechanisms are presented in the figure 4. More than half of the events (57 %) are thrust faults and strike-slip reverse faults, one third (31 %) – strike-slip and overthrust faults, normal and oblique-slip faults are not numerous (12 %). Based on the geological indicators of the Northern Tien Shan the common (averaged) neotectonic stresses, differing for uplifts and depressions, were reconstructed [Sim et al., 2014]. It has been noted, that positive structures deforming within the latest phase occurs in the thrust fault field with a horizontal meridional orientation of the compression axis and the subvertical tension axis. In depressions it occurs in the normal fault field with the vertical subhorizontal tension axis, oriented to the north-northeast.

On the base of analysis of the focal mechanisms of earthquakes in the Northern and Central Tien Shan it has been noted [Krestnikov et al., 1987, Yunga, 1990] that diversity of the source mechanisms is typical for the studied territory, and the most frequent focal mechanisms are thrust, oblique-slip and normal.

Figure 5 a, b represents the distribution diagrams of directions (azimuths) of the compression  $P$  and tension  $T$  axes. Quantitative dependences on the dip angle of these axes are shown in the figure 5 c. The azimuths value has been averaged with a step of  $5^\circ$  for dependences construction, and dip angles value – with a step of  $10^\circ$ . Most of the compression axes have an azimuth of  $340^\circ$ , that corresponds to north-northwestern direction, and the major part of these axes is in the sector of  $330^\circ$ – $360^\circ$ , azimuths of the tension axes do not have a pronounced maximum. Such direction of the compression axes is also noted by other researchers for the Tien Shan region [Krestnikov et al., 1987; Yunga, 1990;

Kurskeev, 2004]. Most of the compression axes have a zero dip angle (subhorizontal position), and the major part of the tension axes has a dip angle close to  $60^\circ$  (subvertical position).

### Dynamic parameters

Working sampling of the dynamic parameters has amounted 150 earthquakes with  $M = 2.8-6$  for 1999–2014 from the SMT catalog. These earthquakes main characteristics (scalar seismic moment, moment magnitude, corner frequency, source radius, stress drop) are presented in the table 1 (see the appendix). The scalar seismic moment and the moment magnitude for these earthquakes are taken from the SMT catalog. The source radius (Brune radius) and the tangential stress drop are calculated.

Together with the dynamic parameters for each earthquake, we have included in the table date, epicenter, depth, energy class, earthquake

magnitude converted from the class  $K$  by the formula [Rautian, 1960], as well as number of seismograms, on which the SMT solution has been obtained. Dependences of the corner frequency  $f_0$ , the scalar moment  $M_0$ , the source radius  $r$  and the stress drop on energy characteristics are shown in the figures 6–8. We have chosen the magnitude  $M$ , converted from the class  $K$ , as energy characteristics, and the moment magnitude  $M_w$ , determined when the seismic moment tensor calculating. For all considered dependences the correlation factors are determined, their values are specified in the figures.

The corner frequency for considered class of events ( $M = 2.8-6$ ) varies from 0.1 to 8.9 Hz (fig. 6), that corresponds to the rupture time in a source 1–0.11 s. The corner frequency  $f_0$  and the scalar seismic moment  $M_0$ , from which the moment magnitude  $M_w$  is determined, are

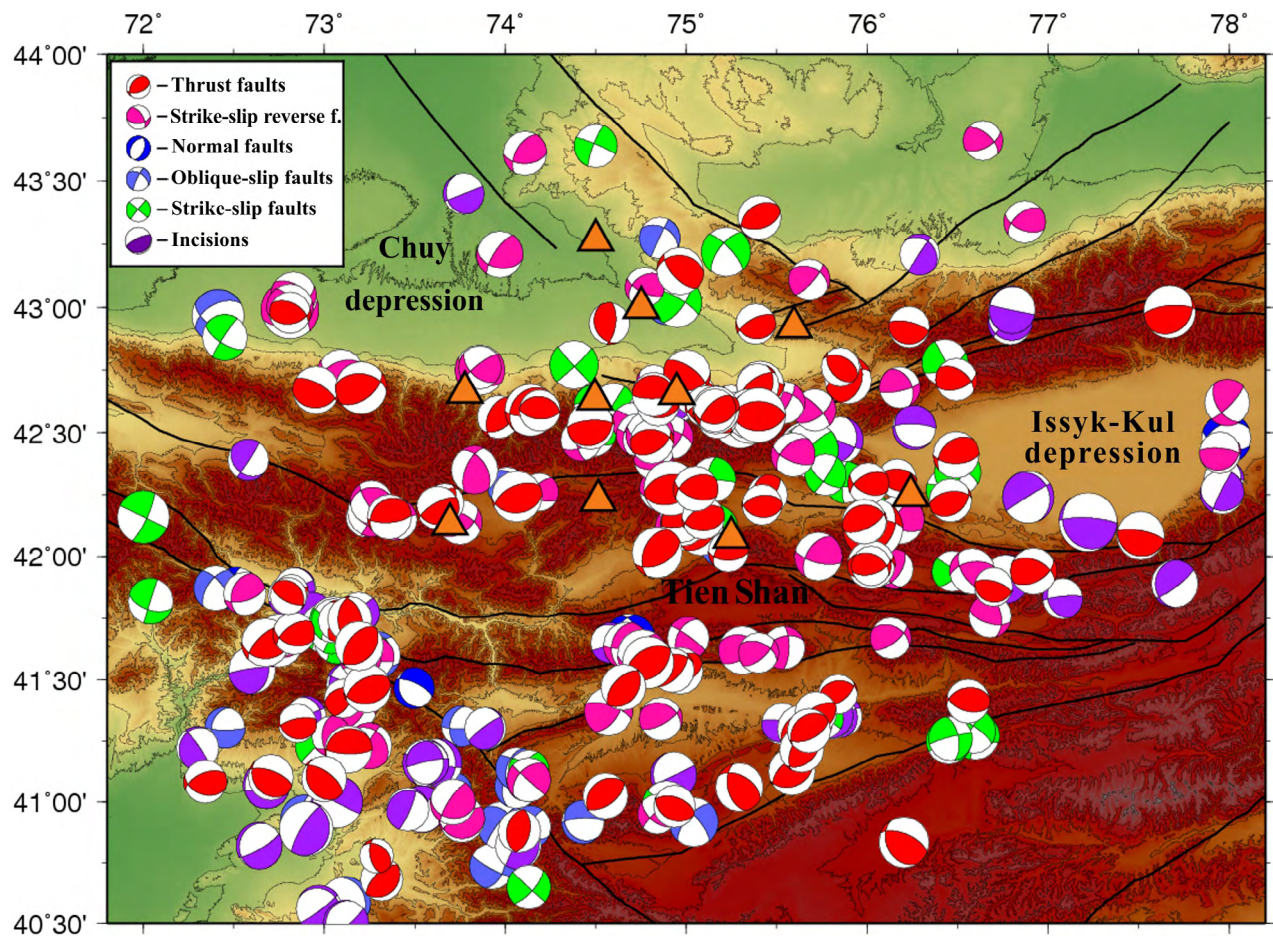


**Figure 4.** Epicenter location and the focal mechanisms of earthquake sources from the catalog of seismic moment tensors (284 events). The KNET stations are designated with the triangles.

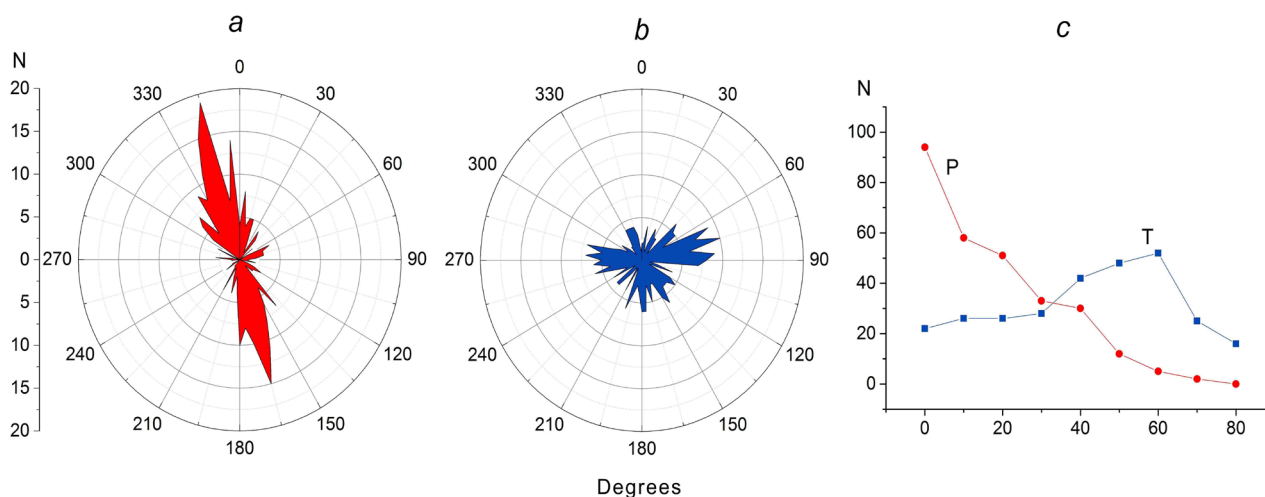


**Figure 5.** Distribution of: a – azimuths of the compression axes  $P$ ; b – azimuths of the tension axes  $T$ ; c – dip angle values of both compression and tension axes.

obtained in the different studies. Nevertheless, distribution of the corner frequency depending on the  $M_w$  is described with a linear model better than that depending on the  $M$ . The variance value of distribution of the deviations from a linear model for the magnitude  $M$  amounts  $D = 389$ , and for the magnitude  $M_w - 322$ .

The scalar seismic moment for the considered class of events varies within the range from  $2.03 \cdot 10^{13}$  to  $4.3 \cdot 10^{17}$  N·m.  $M_0$  dependence on  $M$  is described well with a linear model with positive dip angle: the higher is the magnitude, the higher the value of the scalar seismic moment (fig. 7). This depend-

ence can be described with the expression  $\lg(M_0) = 10.6 + 1.03M$ , that fully corresponds to the expression  $\lg(M_0) = 8.4 + 1.6M$  from the work [Riznichenko, 1985] (where  $M_0$  represented in N·m), and also to the expression, obtained for the earthquakes of the Northern Tien Shan  $\lg(M_0) = 10.1 + 1.1M$  [Sycheva, Bogomolov, 2016]. Values deviation relative to the trend line has lowest variance for the events with  $M > 4.5$ . Dependence of  $\lg(M_0)$  on  $M_w$  is a linear function, as the moment magnitude is determined from the seismic moment and directly depends on it [Kanamori, 1977].

The source radius (Brune radius) for the studied events varies from 150 to 1280 m.

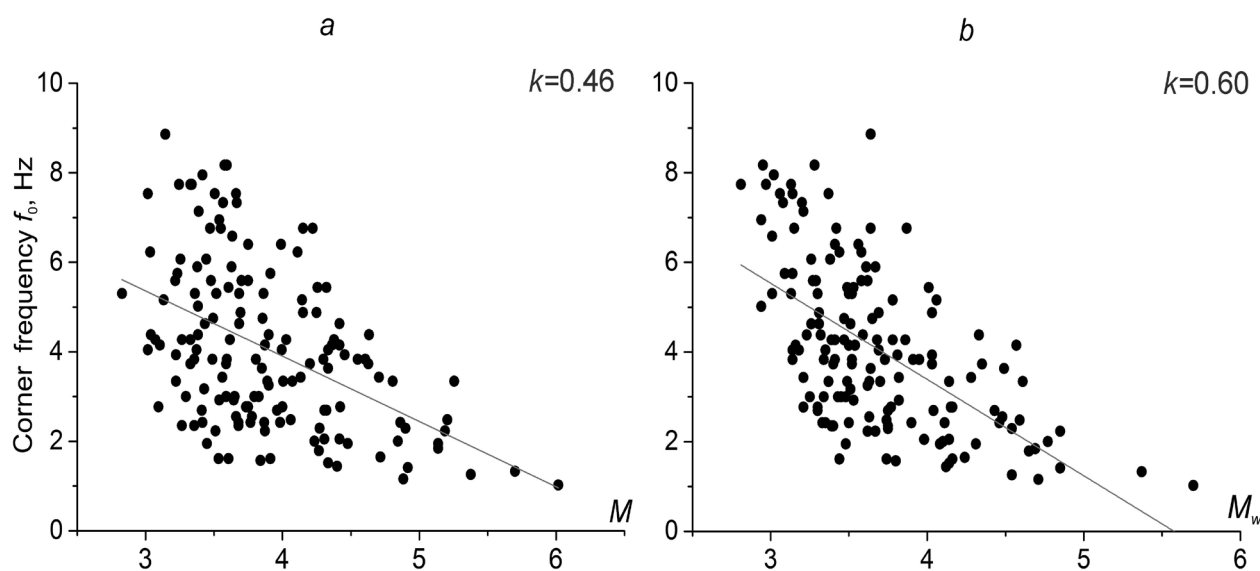


**Figure 6.** The corner frequency  $f_0$  dependence on the magnitude  $M$ , determined by the earthquake class (a), and the moment magnitude  $M_w$  (b).

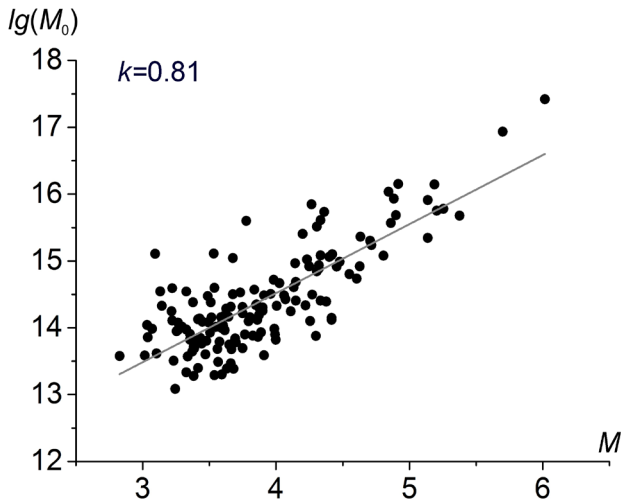


**Figure 7.** Dependence of the scalar seismic moment logarithm on the magnitude  $M$ , determined by the earthquake  $K$ -class.

The Brune radius dependence on  $M$  is presented in the figure 8 a, and on  $M_w$  – in the figure 8 b. Direct relation between the Brune radius and the

corner frequency (equation (1)) is also reflected in presented distributions: dispersion of the values of the Brune radius depending on the  $M_w$  is less than depending on  $M$ .

According to the table 1 (see the appendix) *the stress drop*, varies from  $\sim 0.2$  to  $\sim 130$  MPa. Dependences of stress drop distribution on two magnitudes ( $M$  and  $M_w$ ) are presented in the figure 8 c and 8 d: the stress drop dependence on  $M_w$  has lowest dispersion than on  $M$ , that is also explained with theoretical relation of the stress drop with the Brune radius and the scalar seismic moment.

Analysis of the factor of considered dependences correlation has shown its value to be higher for the moment magnitude  $M_w$  than for the  $M$ . High correlation level (0.81) is obtained for the scalar seismic moment, and the least one – for the stress drop (0.43, 0.62 – for  $M$

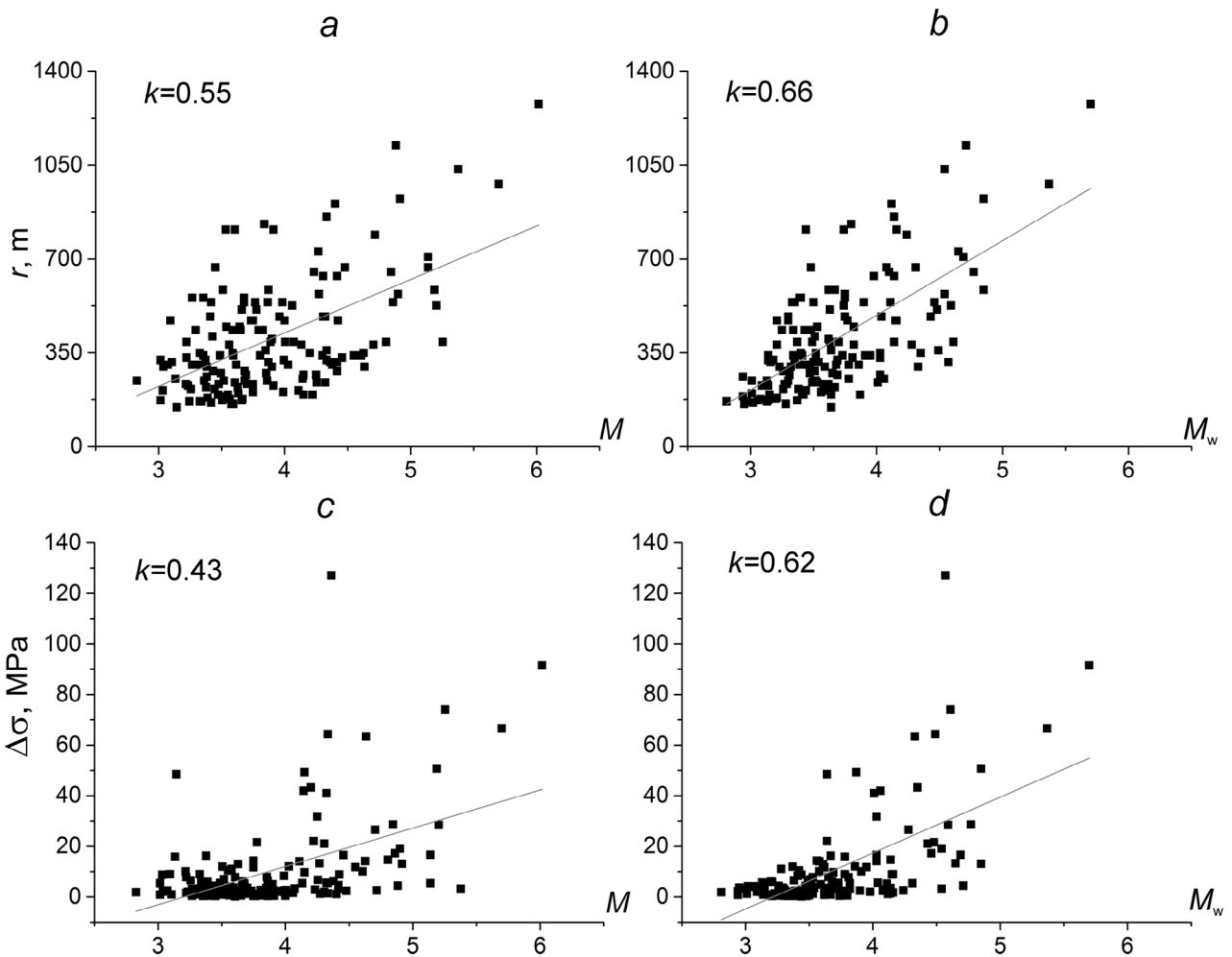


**Figure 8.** The radius  $r$  (a, b) and the stress drop  $\Delta\sigma$  (c, d) dependences on the magnitude  $M$ , determined from the earthquake class  $K$  (a, c), and the moment magnitude  $M_w$  (b, d).

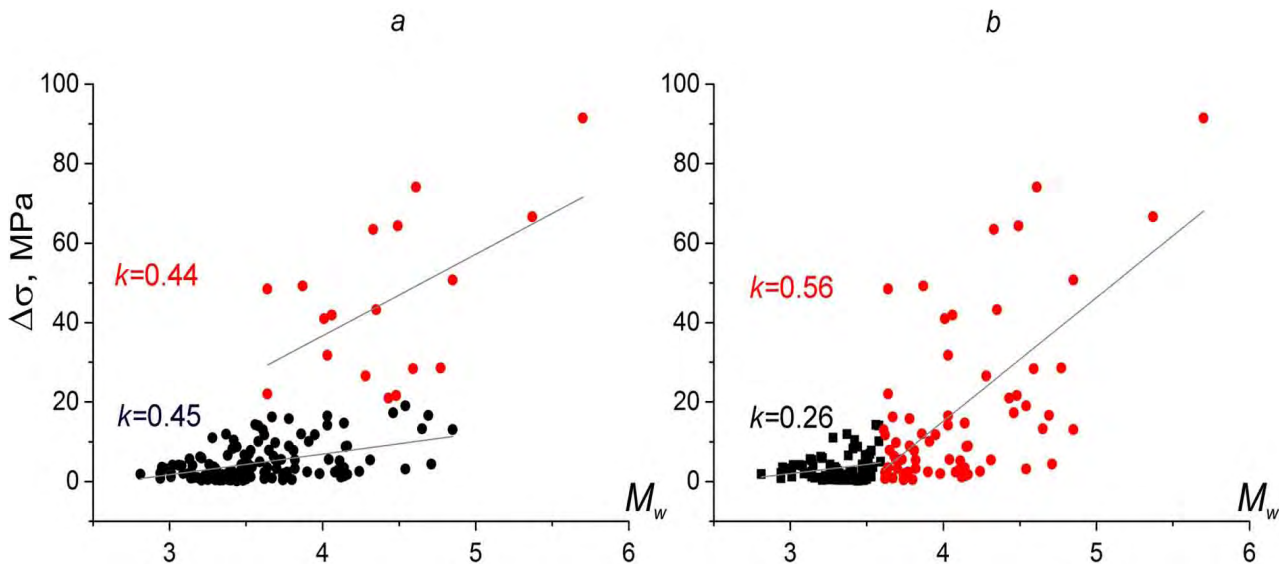


**Figure 9.** The stress drop distribution dependences on magnitude for the earthquakes: a – with  $\Delta\sigma < 20$  MPa (black) and with  $\Delta\sigma \geq 20$  MPa (red); b – with  $M_w < 3.6$  (black) and with  $M_w \geq 3.6$  (red).

and  $M_w$  respectively), that may point to weak relation between this characteristic and the magnitude of event. The value of correlation factor is a little higher for the source radius (0.55, 0.66).

Dependence of the stress drop distribution on the magnitude  $M_w$  is presented in the figure 9. Besides, we separately consider and describe by a linear model the events samplings with  $\Delta\sigma < 20$  MPa and  $\Delta\sigma \geq 20$  MPa (fig. 9 a), as well as dependences of the stress drop  $\Delta\sigma$  for the events with  $M_w < 3.6$  and  $M_w \geq 3.6$  (fig. 9 b). In the graphs the value of the correlation factor of considered dependences is also presented. The samplings, marked in the figure 9 with black color, are described by a linear model with small angle factor, i.e. the stress drop has slightly variable values within the considered range of the magnitudes. Linear models describing the samplings and marked with red have greater angle factor. However, there is a significant dispersion of values on both sides of the model line within the considered range. The correlation factor of the stress drop and moment magnitude for the considered samplings has low values, that may testify to small dependence of the stress drop on the earthquake magnitude.

*Lode–Nadai factor distribution and the stress drop.* In order for gaining an idea of the deformation of the Earth crust as a whole, the Lode–Nadai factor  $\mu_e$  is used. It does not depend

on the tensor's coordinate representation and may be considered as its invariant characteristic. It is worth noting, that, according to [Filin, 1975], when  $\mu_e = 1$  the deformation has a form of a simple compression (uniaxial compression) (when  $\mu_e > 0$  the compressive deformation prevails), when  $\mu_e = -1$  the deformation has a form of a simple tension (uniaxial tension) (when  $\mu_e < 0$  the tensile deformation prevails), when  $\mu_e = 0$  the deformation has a form of a simple shear (pure shear). The figure 10 shows the distribution of the Lode–Nadai factor  $\mu_e$ , calculated on the grounds of the focal mechanisms of earthquakes sources from the SMT catalog (see the figure 4, 284 events) by the methodology, described in the works [Yunga, 1990; Sycheva, Mansurov, 2017].

According to the figure 10, the major part of the studied territory is characterized by the deformation with domination of triaxial state between the pure shear and uniaxial compression ( $\mu_e > 0.2$ ). High value of this factor is typical for the central and eastern parts of the Kyrgyz Range, western part of the Terskey and Kungay Alatau surrounding the Issyk-Kul depression, the Kochkor depression area, the eastern part of the At-Bashy Range, the Naryn-Tau and the central part of the Talas-Fergana Fault. In the western part of the Kyrgyz Range,

the deformation zone with domination of triaxial state between the pure shear and uniaxial tension ( $\mu_e < -0.2$ ) is located. Also, in the studied territory the zones of a pure shear (depressions, see the figure 10) are distinguished. They alternate with mentioned above deformation regimes in the zone parallel with the Talas-Fergana Fault and extended from south to north.

On the same map we marked the mechanisms of sources of 150 earthquakes of 1999–2014 with  $M = 2.8–6$ , for which the dynamic parameters had been calculated. The focal mechanisms of the earthquakes are marked with different colors depending on the value of the stress drop (see explanation to the figure 10). The major part of the «colored» events has thrust focal mechanism, and the minor part – strike-slip reverse mechanism. Significant stress drop is observed in the central part of the Talas-Fergana Fault,

at the end-areas of the Baibiche-Tau Range, in the eastern part of the Moldo Too Range, in the foothills of the western part of the Kyrgyz Range and in its eastern margin, as well in the western part of the Terskey and Kungey Alatau ranges. Absence of the stress drop is marked in a joint zone of the Kyrgyz Range and Chuy depression from  $74.5^\circ$  to  $75.5^\circ$  E. The same area of the significant stress drop absence is distinguished in the work [Sycheva, Bogomolov, 2016]. The most of events with  $\Delta\sigma \geq 10$  are located in the zones, characterized by deformation with domination of triaxial state between the pure shear and uniaxial compression. The events with  $\Delta\sigma < 1$  MPa and  $1 \leq \Delta\sigma < 10$  are mostly located in the same areas. The events with  $\Delta\sigma \geq 10$  MPa are absent in the Suusamyр depression and its vicinity. It indicates possibly that the stress drop occurred in this area as a result of the Suusamyр

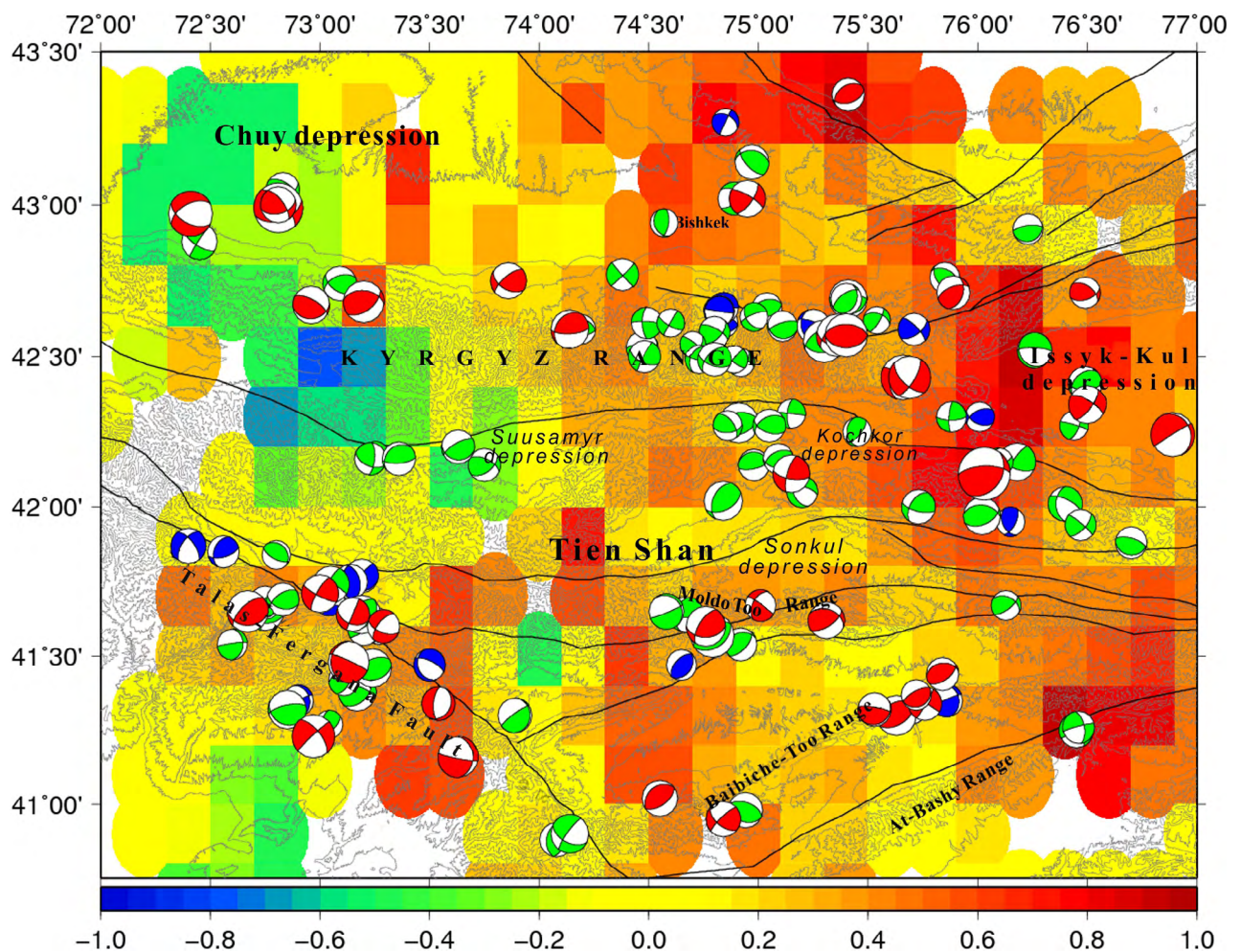


**Figure 10.** The Lode–Nadai factor  $\mu_e$  distribution and epicentral location of 150 events of 1999–2014 with  $M = 2.8–6$  (table 1, see the appendix) and their focal mechanisms. Red color of the focal mechanism – the earthquakes with  $\Delta\sigma \geq 10$  MPa (40 events), green –  $1 \leq \Delta\sigma < 10$  MPa (87 events), blue –  $\Delta\sigma < 1$  MPa (23 events). The regional faults are marked with black lines.

earthquake (19.08.1992,  $M = 7.3$ ). In the work [Sychev et al., 2019] the earthquakes catalogue and aftershock sequence of the Suusamyр earthquake have been considered in the context of nonequilibrium thermodynamics with using the Tsallis statistics, generalizing the classic Boltzmann-Gibbs statistics [Tsallis, 1988; Chelidze et al., 2018]. The differences in  $q$ -parameter of the Tsallis statistics have been revealed before and after the Suusamyр earthquake. Also, an abrupt increase of cross-correlations took place in the studied region before the main shock, with the sharp decrease immediately after it, and further return to the average value, observed before the mainshock.

### Conclusion

Based on the waveform inversion method, we determined the seismic moment tensors for 177 earthquakes with  $K \geq 10.5$ , occurred from 2007 to 2017 in the territory of the Central Tien Shan. Obtained solutions have been included in the SMT catalog. The final catalogue includes the parameters of 284 events, occurred in 1996–2017. Some its characteristics are presented. The diagrams of the azimuths of principal stresses axes are constructed: the major part of compression axes falls in the sector with a direction of  $330$ – $360^\circ$ , most of them have an angle of  $340^\circ$ , the azimuths of tension axes do not have an explicit maximum. The dominant part of compression axes is characterized with near-horizontal position and tension axes – with near-vertical one. A majority of earthquakes occurred in the studied territory are of thrust and strike-slip reverse type of fault, and the minority – strike-slip faults and incisions. Only small fraction of the events has a normal and oblique-slip type of focal mechanism.

For the 150 earthquakes with  $M = 2.8$ – $6$  from the seismic moment tensors catalogue the dynamic parameters have been calculated: the source radius  $r$  and the stress drop  $\Delta\sigma$ . The dependences of the scalar moment distribution, the source radius and the stress drop on the magnitude  $M$  converted from the class  $K$ , and the moment magnitude  $M_w$  have been constructed. The correlation coefficients of the dynamic parameters and the moment magnitude are higher than that of the dynamic parameters and the magnitude converted from the class. Weaker correlation takes place between the stress drop  $\Delta\sigma$  and the magnitude in comparison with the correlation between the scalar seismic moment and the magnitude, as well as between the source radius and the magnitude.

The Lode–Nadai factor  $\mu_\varepsilon$  distribution, constructed on the base of the seismic moment catalogue, demonstrates that the most part of the studied territory is in the conditions of deformation with triaxial state between the pure shear and uniaxial compression domination ( $\mu_\varepsilon > 0.2$ ), in the north-western part the deformation area with of triaxial state between the pure shear and uniaxial tension domination ( $\mu_\varepsilon < -0.2$ ) is distinguished, for the major part of the depressions the pure shear deformation ( $-0.2 \leq \mu_\varepsilon \leq 0.2$ ) is typical. Values of the Lode–Nadai factor are compared with values of the stress drop  $\Delta\sigma$  for the 150 earthquakes. The significant stress drop is character for the areas with the deformation of a simple compression prevailing. Absence of the significant stress drop in the territory of the Suusamyр depression and its vicinity is noted. This may be a signature of nonlocal stress unloading resulted from the Suusamyр earthquake (19.08.1992,  $M = 7.3$ ) and its aftershocks (more than 2000).

## Appendix / Приложение

Table 1. Some parameters of the 150 earthquakes of 1999–2014,  $M = 2.8–6$  and their dynamic parametersТаблица 1. Характеристики 150 землетрясений 1999–2014 гг. с  $M = 2.8–6$  и их динамические параметры

№	Date	Time	$\varphi^\circ$	$\lambda^\circ$	H, km	K	M	$M_0, 10^{14}$ N·m	$M_w$	$f_0$ , Hz	r, m	$\Delta\sigma$ , MPa	$N_{obs}$
1	14.04.1999	12:41:22.19	43.64	74.50	15.90	10.66	03.70	1.01	3.27	5.59	233	3.48	6
2	24.05.1999	07:39:21.39	42.66	75.04	06.80	10.65	03.69	1.15	3.31	4.88	267	2.64	7
3	13.02.2000	09:46:07.60	41.71	73.00	04.10	12.02	04.46	13.8	4.03	3.93	332	16.52	7
4	01.07.2000	20:33:58.86	41.16	73.63	00.00	11.75	04.31	54.6	4.43	2.69	485	21.00	10
5	14.07.2000	08:22:46.84	41.38	73.17	00.10	10.62	03.68	18.5	4.11	2.42	539	5.17	13
6	28.07.2000	08:56:26.91	42.58	74.80	16.20	11.19	03.99	1.32	3.35	4.04	323	1.72	15
7	08.08.2000	01:15:07.58	42.24	76.89	00.20	12.72	04.84	181.0	4.77	2.00	652	28.56	8
8	02.03.2001	06:18:30.26	40.88	74.08	00.00	10.62	03.68	5.28	3.75	2.35	555	1.35	7
9	10.04.2001	00:13:24.43	41.77	73.19	00.00	10.32	03.51	4.01	3.67	2.23	585	0.88	10
10	09.05.2001	11:14:16.23	41.74	73.08	00.00	10.04	03.36	1.34	3.40	2.35	555	0.34	19
11	22.05.2001	15:02:33.55	42.15	76.18	13.20	12.06	04.48	16.1	4.08	1.95	668	2.36	17
12	08.07.2001	11:51:52.68	42.14	74.98	14.10	11.18	03.99	1.60	3.41	6.40	204	8.27	10
13	18.08.2001	01:12:04.20	42.17	73.25	05.80	10.04	03.36	1.10	3.14	3.83	340	1.22	7
14	20.08.2001	01:27:05.74	42.14	74.98	06.90	10.47	03.59	1.64	3.41	3.83	340	1.82	11
15	13.09.2001	12:00:30.35	41.30	75.63	00.90	11.56	04.20	42.2	4.35	3.73	349	43.25	8
16	09.10.2001	00:24:30.84	42.01	76.40	00.00	11.31	04.06	5.07	3.74	2.48	526	1.53	8
17	18.11.2001	01:28:55.44	42.59	74.14	06.50	12.65	04.81	20.0	4.14	3.34	390	14.70	15
18	26.02.2002	01:37:22.48	42.74	73.09	00.00	11.47	04.15	4.23	3.69	4.88	267	9.72	11
19	28.03.2002	22:36:21.12	41.60	73.29	05.20	11.40	04.11	2.94	3.58	6.23	209	14.04	14
20	17.06.2002	21:03:47.98	42.14	73.75	07.90	10.97	03.87	2.56	3.54	4.15	314	3.62	14
21	31.08.2002	17:46:38.13	41.59	73.27	10.00	10.41	03.56	0.80	3.21	3.43	380	0.64	8
22	27.10.2002	01:26:38.65	42.92	76.23	07.00	10.26	03.48	1.05	3.29	5.59	233	3.64	6
23	08.12.2002	22:10:39.77	41.87	72.40	00.10	10.91	03.84	6.20	3.80	1.57	830	0.47	11
24	21.02.2003	10:35:22.15	42.53	74.47	13.10	11.66	04.26	2.10	3.49	5.44	240	6.68	8
25	09.03.2003	00:32:05.75	41.23	72.97	00.10	11.68	04.27	1.17	4.65	1.79	728	13.27	19
26	22.05.2003	18:11:55.01	42.99	72.81	07.00	14.26	05.70	1.43	5.37	1.33	980	66.60	14
27	22.05.2003	19:03:57.95	42.99	72.82	05.70	11.02	03.90	3.33	3.62	3.25	401	2.26	5
28	22.05.2003	19:34:47.18	43.06	72.83	06.60	11.21	04.01	3.53	3.63	3.34	390	2.60	10
29	23.05.2003	00:16:04.86	43.00	72.81	06.40	11.47	04.15	8.07	3.87	6.76	193	49.24	14
30	25.05.2003	22:44:22.26	42.98	72.81	12.20	10.14	03.41	1.11	3.30	2.69	485	0.43	9
31	28.07.2003	04:57:29.84	41.64	74.67	02.80	11.44	04.13	6.75	3.82	3.43	380	5.38	16
32	26.08.2003	18:58:17.38	40.98	74.94	00.90	10.37	03.54	6.59	3.82	2.92	446	3.24	11
33	06.10.2003	02:51:34.14	41.25	76.45	00.00	11.13	03.96	5.34	3.75	2.69	485	2.05	12
34	06.10.2003	16:42:13.93	42.50	74.48	16.40	11.95	04.42	2.19	3.50	4.15	314	3.09	13
35	18.11.2003	06:49:56.55	41.26	76.46	00.00	10.83	03.79	2.07	3.48	3.00	434	1.11	9
36	16.01.2004	09:06:17.90	42.55	75.30	14.00	13.68	05.38	79.2	4.54	1.26	1035	3.13	17

№	Date	Time	$\varphi^\circ$	$\lambda^\circ$	H, km	K	M	$M_0, 10^{14}$ N·m	$M_w$	$f_0$ , Hz	r, m	$\Delta\sigma$ , MPa	$N_{obs}$
37	25.04.2004	04:15:18.19	41.54	74.93	15.50	10.85	03.81	2.39	3.52	3.83	340	2.65	10
38	02.06.2004	17:15:10.82	42.28	74.91	17.90	13.25	05.14	36.7	4.31	1.95	668	5.38	16
39	02.08.2004	18:20:11.89	41.35	72.90	00.60	09.88	03.27	1.54	3.39	2.35	555	0.39	6
40	26.08.2004	20:23:22.86	41.85	72.56	00.00	10.49	03.61	1.80	3.44	1.61	810	0.15	6
41	15.10.2004	13:45:56.82	41.02	74.56	00.00	11.25	04.03	7.78	3.86	4.27	305	11.97	8
42	27.11.2004	12:42:54.30	42.61	74.84	15.10	10.57	03.65	0.93	3.25	3.00	434	0.50	14
43	29.11.2004	00:44:54.94	41.62	75.31	17.00	11.78	04.32	12.9	4.01	5.44	240	40.99	19
44	20.04.2005	17:48:53.10	42.41	76.49	06.70	11.33	04.07	4.43	3.70	3.34	390	3.26	13
45	08.06.2005	21:05:21.44	42.16	75.09	17.20	10.63	03.68	0.98	3.26	4.63	282	1.93	8
46	20.06.2005	14:25:01.50	42.77	74.38	23.30	11.95	04.42	2.33	3.51	4.63	282	4.56	14
47	05.07.2005	03:07:24.82	41.60	74.76	18.40	12.47	04.71	33.3	4.28	3.43	380	26.53	6
48	07.07.2005	19:22:05.42	42.66	74.84	11.90	10.89	03.83	1.27	3.34	3.00	434	0.68	9
49	07.07.2005	21:00:07.50	42.65	74.82	11.00	10.78	03.77	1.32	3.35	2.42	539	0.37	12
50	03.10.2005	09:28:26.24	42.65	74.82	11.90	10.75	03.75	0.82	3.21	2.77	471	0.35	8
51	08.10.2005	06:25:58.93	42.10	76.05	06.80	12.34	04.63	38.2	4.33	4.38	298	63.48	13
52	27.12.2005	00:55:30.54	42.71	75.89	06.20	11.60	04.22	3.60	3.64	6.76	193	21.99	12
53	28.12.2005	01:52:48.29	42.69	75.41	12.50	11.92	04.40	19.2	4.12	1.44	905	1.13	12
54	29.12.2005	08:50:32.76	42.69	75.39	06.40	10.51	03.62	1.5	3.39	4.27	305	2.35	8
55	01.01.2006	08:56:53.85	42.60	75.25	22.20	10.97	03.87	3.36	3.62	2.23	585	0.73	6
56	27.03.2006	09:49:33.57	42.16	73.23	00.00	09.88	03.27	1.98	3.47	4.27	305	3.05	9
57	24.05.2006	13:17:54.27	42.67	72.96	12.60	11.65	04.25	13.8	4.03	4.88	267	31.73	19
58	12.06.2006	17:53:49.37	41.44	75.84	01.20	09.79	03.22	2.93	3.58	5.59	233	10.10	11
59	08.07.2006	18:58:20.37	41.61	73.25	13.50	10.46	03.59	2.39	3.52	3.73	349	2.45	8
60	13.07.2006	10:09:30.85	42.76	75.85	11.10	09.47	03.04	1.19	3.32	4.38	298	1.98	5
61	22.07.2006	05:08:23.35	41.67	76.13	07.40	10.09	03.38	0.87	3.23	4.38	298	1.44	7
62	24.07.2006	15:53:48.77	41.64	73.15	08.30	10.53	03.63	3.20	3.61	5.90	221	12.96	7
63	30.07.2006	11:48:16.11	41.65	72.67	03.00	11.80	04.33	68.1	4.49	3.63	359	64.34	11
64	30.07.2006	13:13:40.61	41.67	72.78	00.00	10.05	03.36	1.10	3.30	5.30	246	3.24	7
65	13.08.2006	06:10:13.41	41.65	72.75	00.00	11.95	04.42	20.4	4.14	2.05	636	3.47	17
66	15.08.2006	18:58:22.87	42.60	75.11	10.20	10.18	03.43	1.17	3.31	4.63	282	2.28	10
67	18.08.2006	15:41:10.87	41.67	72.75	00.00	10.56	03.64	2.43	3.53	2.92	446	1.19	7
68	29.08.2006	07:54:16.36	41.69	72.83	00.00	10.33	03.52	2.36	3.52	5.30	246	6.95	5
69	22.10.2006	11:01:32.21	42.16	73.36	06.60	10.93	03.85	3.64	3.64	3.63	359	3.43	9
70	08.11.2006	02:21:26.94	42.56	75.36	18.60	13.37	05.21	94.20	4.59	2.48	526	28.37	21
71	08.11.2006	02:26:50.84	42.57	75.35	20.10	10.94	03.86	3.70	3.65	4.75	274	7.84	4
72	25.12.2006	20:00:58.32	42.11	76.03	00.10	14.83	06.02	4370.0	5.70	1.02	1278	91.51	12
73	02.01.2007	04:06:54.03	42.31	77.97	00.40	09.99	03.33	5.80	3.78	4.27	305	8.91	6
74	02.03.2007	12:57:05.93	41.27	73.04	01.60	09.82	03.23	0.54	3.09	5.75	227	2.01	4
75	20.03.2007	03:17:54.83	41.34	73.54	04.60	10.75	03.75	3.39	3.62	5.59	233	11.70	4

**SEISMIC MOMENT TENSOR AND DYNAMIC PARAMETERS OF EARTHQUAKES IN THE CENTRAL TIEN SHAN**

№	Date	Time	$\varphi^\circ$	$\lambda^\circ$	H, km	K	M	$M_0, 10^{14}$ N·m	$M_w$	$f_0$ , Hz	r, m	$\Delta\sigma$ , MPa	$N_{obs}$
76	27.05.2007	01:30:53.75	41.74	73.05	14.40	11.75	04.31	11.6	3.98	2.05	636	1.98	18
77	06.06.2007	11:09:25.58	42.57	75.40	13.00	13.25	05.14	135.0	4.69	1.84	708	16.65	21
78	09.10.2007	16:00:41.39	42.98	77.67	00.00	12.82	04.90	80.3	4.54	2.29	569	19.05	7
79	21.10.2007	14:08:44.42	42.57	75.35	13.60	10.96	03.87	1.21	3.33	2.42	539	0.34	7
80	04.01.2008	15:38:16.48	43.36	75.41	07.00	10.75	03.75	2.76	3.56	6.40	204	14.27	6
81	08.01.2008	18:04:13.75	42.05	75.20	16.80	11.00	03.89	1.42	3.37	3.34	390	1.04	5
82	12.01.2008	01:53:05.09	43.28	74.85	13.00	10.09	03.38	0.32	2.94	5.02	260	0.79	6
83	30.01.2008	15:28:43.39	41.63	73.19	11.20	10.29	03.49	2.01	3.47	4.75	274	4.26	7
84	03.02.2008	04:57:07.55	41.94	76.47	00.00	09.99	03.33	1.57	3.40	3.73	349	1.61	8
85	04.04.2008	07:21:26.61	41.54	72.60	10.00	41.80	21.00	1.26	3.34	3.83	340	1.40	7
86	25.06.2008	21:09:29.86	41.30	73.89	00.70	10.28	03.49	4.96	3.73	3.83	340	5.50	18
87	19.08.2008	19:52:39.54	41.32	75.70	00.10	09.43	03.02	0.64	3.14	4.04	323	0.83	6
88	21.08.2008	17:19:51.67	41.97	76.02	14.20	11.78	04.32	14.4	4.04	2.69	485	5.52	19
89	20.09.2008	04:15:52.27	42.27	74.86	21.70	10.60	03.67	0.80	3.20	7.33	178	6.20	4
90	19.10.2008	01:27:14.11	41.34	75.76	07.10	09.66	03.14	3.53	3.64	8.86	147	48.47	3
91	02.11.2008	17:58:26.98	42.71	76.49	04.10	10.31	03.51	1.41	3.37	7.53	173	11.92	5
92	03.12.2008	04:26:28.64	42.68	73.20	11.00	12.75	04.86	61.7	4.46	2.42	539	17.27	19
93	22.01.2009	12:55:14.19	42.61	74.49	16.90	09.86	03.26	1.48	3.38	6.07	215	6.54	4
94	01.02.2009	11:25:38.02	42.75	73.86	14.90	12.29	04.61	9.07	3.91	3.83	340	10.06	15
95	27.04.2009	20:04:12.18	42.97	72.41	08.80	12.85	04.92	236.0	4.85	1.41	924	13.06	11
96	05.05.2009	06:19:05.59	41.47	73.50	00.00	09.93	03.29	1.73	3.43	3.00	434	0.92	7
97	16.05.2009	05:38:46.20	42.59	74.19	06.00	10.10	03.39	0.82	3.21	7.14	183	5.89	7
98	24.05.2009	00:08:40.93	42.61	74.60	12.60	10.54	03.63	0.41	3.01	6.58	198	2.30	11
99	25.07.2009	14:57:10.42	42.58	75.71	12.10	10.46	03.59	1.85	3.45	3.00	434	0.99	8
100	07.08.2009	04:32:46.39	42.01	75.72	05.60	11.80	04.33	4.22	3.69	4.04	323	5.49	7
101	24.09.2009	07:57:10.94	42.08	77.51	08.20	11.85	04.36	90.0	4.57	4.15	314	127.10	5
102	11.10.2009	06:25:45.82	43.14	74.97	20.10	11.69	04.27	5.21	3.75	2.29	569	1.24	4
103	02.11.2009	19:46:34.03	41.67	75.01	17.80	10.39	03.55	1.71	3.42	6.76	193	10.41	3
104	07.12.2009	18:05:51.07	41.35	75.86	00.00	10.15	03.42	2.22	3.50	2.42	539	0.62	13
105	22.12.2009	05:54:31.37	41.75	73.14	00.10	11.04	03.91	5.09	3.74	1.61	810	0.42	15
106	24.12.2009	02:15:46.95	42.88	72.45	14.40	11.17	03.98	8.72	3.90	2.42	539	2.44	7
107	02.03.2010	01:55:36.02	42.43	75.66	19.30	13.34	05.19	232.0	4.85	2.23	585	50.71	16
108	02.03.2010	04:17:40.13	42.44	75.65	19.90	10.95	03.86	2.18	3.50	5.30	246	6.42	9
109	03.06.2010	10:36:14.15	41.88	76.70	02.40	09.46	03.03	1.83	3.44	6.23	209	8.73	10
110	24.07.2010	04:19:32.96	41.42	73.11	00.20	09.53	03.07	1.60	3.41	4.27	305	2.46	5
111	09.09.2010	18:31:50.35	42.31	75.15	18.80	11.04	03.91	0.65	3.14	5.75	227	2.42	8
112	20.09.2010	09:07:15.09	41.59	73.19	12.20	10.17	03.43	2.28	3.51	3.17	411	1.43	4
113	29.09.2010	07:30:07.97	42.25	75.45	17.10	10.01	03.34	0.62	3.13	7.74	168	5.65	4
114	27.10.2010	04:48:02.87	41.46	73.24	10.80	11.80	04.33	20.2	4.14	1.52	858	1.40	24
115	19.12.2010	19:12:48.85	42.54	74.70	06.90	09.84	03.24	0.20	2.81	7.74	168	1.86	5

№	Date	Time	$\varphi^\circ$	$\lambda^\circ$	H, km	K	M	$M_0, 10^{14}$ N·m	$M_w$	$f_0$ , Hz	r, m	$\Delta\sigma$ , MPa	$N_{obs}$
116	18.03.2011	09:36:26.66	43.02	74.95	16.30	12.19	04.55	10.6	3.95	3.83	340	11.74	17
117	23.03.2011	20:19:43.71	43.02	74.89	18.50	10.49	03.61	2.45	3.53	5.44	240	7.79	7
118	09.04.2011	12:30:24.93	42.02	74.84	20.60	12.49	04.72	29.0	4.24	1.65	790	2.57	21
119	02.12.2011	00:24:02.64	42.52	76.26	00.10	10.72	03.73	5.62	3.77	2.77	471	2.36	11
120	16.12.2011	03:14:40.13	42.30	75.88	13.20	10.20	03.44	0.97	3.26	6.07	215	4.28	8
121	24.12.2011	09:20:07.10	41.64	73.19	11.20	11.96	04.42	21.0	4.15	2.77	471	8.80	12
122	05.02.2012	07:10:18.06	41.57	74.79	17.10	12.79	04.88	142.0	4.71	1.16	1124	4.39	21
123	10.02.2012	06:49:17.11	42.94	74.57	15.80	10.15	03.42	0.42	3.02	7.95	164	4.12	9
124	19.02.2012	05:23:03.04	43.66	76.64	02.50	09.80	03.22	2.13	3.49	3.34	390	1.57	8
125	20.02.2012	02:23:56.17	41.48	73.13	00.00	10.80	03.78	66.0	4.48	2.55	511	21.61	15
126	20.02.2012	04:18:07.52	41.32	72.85	00.10	09.57	03.09	21.3	4.16	2.77	471	8.93	16
127	28.03.2012	12:54:01.43	42.49	74.73	16.80	10.42	03.57	0.51	3.08	7.33	178	3.97	14
128	16.05.2012	03:26:40.57	42.48	74.92	15.90	10.63	03.68	0.41	3.01	5.30	246	1.19	12
129	27.08.2012	00:24:59.09	41.32	75.53	03.10	10.08	03.38	4.00	3.67	5.90	221	16.24	11
130	29.09.2012	21:35:04.01	41.69	73.04	09.10	10.21	03.45	2.04	3.48	1.95	668	0.30	15
131	14.10.2012	16:30:08.24	40.90	74.14	00.00	10.36	03.53	21.5	4.16	1.61	810	1.77	8
132	15.11.2012	16:07:43.48	41.65	74.58	18.10	09.80	03.22	6.51	3.81	3.93	332	7.80	5
133	28.11.2012	05:30:08.53	41.89	77.70	00.30	11.62	04.23	17.6	4.10	2.00	652	2.78	7
134	29.11.2012	18:18:46.58	40.95	74.84	00.00	09.64	03.13	5.82	3.78	5.16	253	15.80	6
135	04.04.2013	16:07:21.72	42.62	75.54	20.30	10.37	03.54	0.32	2.94	6.95	188	2.15	5
136	02.05.2013	04:52:25.03	42.20	73.63	06.20	10.59	03.66	3.41	3.63	2.55	511	1.12	14
137	06.06.2013	03:03:07.42	42.27	76.43	23.30	10.25	03.47	0.66	3.15	6.76	193	4.05	12
138	24.06.2013	00:59:55.09	42.15	76.10	14.40	09.99	03.33	0.36	2.97	7.74	168	3.27	6
139	15.07.2013	18:19:08.03	42.49	74.89	14.20	10.47	03.59	0.33	2.95	8.17	160	3.58	9
140	25.07.2013	03:39:16.67	41.37	75.72	08.90	10.44	03.58	1.02	3.28	8.17	160	11.01	22
141	20.09.2013	16:28:25.99	42.34	76.50	06.80	11.46	04.14	15.4	4.06	5.16	253	41.90	11
142	21.09.2013	04:03:34.86	41.95	76.15	03.00	09.59	03.11	0.69	3.16	4.15	314	0.97	5
143	17.10.2013	06:19:21.09	42.63	74.98	09.30	10.59	03.66	0.49	3.06	7.53	173	4.11	7
144	23.11.2013	09:42:06.75	42.43	75.69	09.90	13.46	05.26	101.0	4.61	3.34	390	74.12	8
145	21.01.2014	20:46:36.20	42.11	75.14	14.70	12.33	04.63	13.8	4.03	3.73	349	14.16	14
146	14.02.2014	18:43:03.71	42.30	76.01	15.90	10.07	03.37	0.73	3.18	4.04	323	0.95	6
147	22.02.2014	04:24:12.46	41.47	74.65	00.00	47.20	24.00	1.10	3.30	2.77	471	0.46	6
148	27.04.2014	14:04:51.57	41.84	72.80	00.10	09.09	02.83	0.63	3.13	5.30	246	1.84	6
149	13.05.2014	01:18:44.89	42.27	75.05	06.70	11.02	03.90	2.99	3.59	4.38	298	4.96	13
150	28.05.2014	02:25:58.35	42.49	74.80	12.10	11.88	04.38	4.10	3.68	4.27	305	6.30	15

Note.  $\varphi$  – latitude,  $\lambda$  – longitude,  $H$  – depth,  $K$  – class,  $M$  – magnitude,  $f_0$  – corner frequency,  $M_0$  – scalar seismic moment,  $r$  – source radius,  $\Delta\sigma$  – stress drop,  $N_{obs}$  – number of seismograms, on the which base the seismic moment tensor is obtained.

Примечание.  $\varphi$  – широта,  $\lambda$  – долгота,  $H$  – глубина,  $K$  – класс,  $M$  – магнитуда,  $f_0$  – угловая частота,  $M_0$  – скалярный сейсмический момент,  $r$  – радиус очага,  $\Delta\sigma$  – сброс напряжений,  $N_{obs}$  – количество сейсмограмм, на основе которых получен тензор сейсмического момента

## References

1. Abercrombie R.E., Rice J.R. **2005**. Can observations of earthquake scaling constrain slip weakening? *Geophysical J. International*, 162: 406–424. <https://doi.org/10.1111/j.1365-246x.2005.02579.x>
2. Brune J.N. **1970**. Tectonic stress and the spectra of seismic shear waves from earthquakes. *J. of Geophysical Research*, 75(26): 4997–5009. <https://doi.org/10.1029/jb075i026p04997>
3. Brune J.N. **1971**. Corrections. *J. of Geophysical Research*, 76: 5002.
4. Chelidze T. et al. (eds) **2018**. *Complexity of seismic time series: Measurement and application*. Amsterdam, Netherlands: Elsevier, 548 p. <https://doi.org/10.1016/c2016-0-04546-1>
5. Dziewonski A.M., Chou T.-A., Woodhouse J. H. **1981**. Determination of earthquake source parameters from waveform data for studies of global and regional seismicity. *J. of Geophysical Research: Solid Earth*, 86(B4): 2825–2852. <https://doi.org/10.1029/jb086ib04p02825>
6. Eshelby J.D. **1957**. The determination of elastic field of an ellipsoidal inclusion and related problems. *Proceedings of the Royal Society of London*, A241(1226): 376–396. <https://doi.org/10.1098/rspa.1957.0133>
7. Filin A.P. **1975**. [*Applied mechanics of deformable solids*], vol. 1. Moscow: Nauka, 832 p. (In Russ.).
8. Fukahata Yu., Yagi Y., Matsu'ura M. **2003**. Waveform inversion for seismic source processes using ABIC with two sorts of prior constraints: Comparison between proper and improper formulations. *Geophysical Research Letters*, 30. <https://doi.org/10.1029/2002gl016293>
9. *Geologicheskaja karta Kirgizskoi SSR [Geological map of the Kyrgyz SSR]*. **1980**. [On a scale 1 : 500 000]. Ed.-in-Chief S.A. Igemberdiev. Leningrad: MinGeo USSR, 6 sheets. (In Russ.).
10. Kanamori H. **1977**. The energy release in great earthquakes. *J. of Geophysical Research*, 82(20): 2981–2987. <https://doi.org/10.1029/jb082i020p02981>
11. Kikuchi M., Kanamori H. **1991**. Inversion of complex body waves-III. *Bulletin of the Seismological Society of America*, 81(6): 2335–2350.
12. Kocharyan G.G. **2016**. *Geomekhanika razlomov [Geomechanics of faults]*. Moscow: GEOS, 424 p. (In Russ.).
13. Kohketsu K. **1985**. The extended reflectivity method for synthetic nearfield seismograms. *J. of Physics of the Earth*, 33: 121–131. <https://doi.org/10.4294/jpe1952.33.121>
14. Kostyuk A.D. **2008**. [The mechanisms of earthquakes sources of intermediate intensity at the Northern Tien Shan]. *Vestnik Kirgyzsko-Rossiiskogo Slavianskogo universiteta [Vestnik of the Kyrgyz-Russian Slavic University]*, 8(1): 100–105. (In Russ.).
15. Kostyuk A.D., Sycheva N.A., Yunga S.L., Bogomolov L.M., Yagi Y. **2010**. Deformation of the Earth's crust in the Northern Tien Shan according to the earthquake focal data and satellite geodesy. *Izvestiya, Physics of the Solid Earth*, 46(3): 230–243.
16. Krestnikov V.N., Shishkin E.I., Shtange D.V., Yunga S.L. **1987**. [Stressed state of the Earth crust of the Central and Northern Tien Shan]. *Izv. AN SSSR, Fizika Zemli = Izvestiya, Physics of the Solid Earth*, 3: 13–30. (In Russ.).
17. Kurskeev A.K. **2004**. *Zemletriaseniia i seismicheskaja bezopasnost' Kazakhstana [Earthquakes and seismic safety of Kazakhstan]*. Almaty: Evero, 501 p. (In Russ.).
18. Kurskeev A.K., Belosludtsev O.M., Zhdanovich A.R., Serazetdinova B.Z., Stepanov B.S., Uzbekov N.B. **2004**. *Seismologicheskaja opasnost' orogenov Kazakhstana [Seismic hazard for the orogens of Kazakhstan]*. Almaty: Evero, 294 p. (In Russ.).
19. Lay T., Wallace T. (eds) **1995**. *Modern global seismology*. San-Diego: Academic Press, 517 p. (International Geophysics; 58).
20. Madariaga R. **1979**. On the relation between seismic moment and stress drop in the presence of stress and strength heterogeneity. *J. of Geophysical Research*, 84: 2243–2250. <https://doi.org/10.1029/jb084ib05p02243>
21. Puzyrev N.N. **1997**. [*Methods and objects of seismic research*]. Novosibirsk: SO RAN Publ.: NITsOIGGM, 300 p. (In Russ.).
22. Rautian T.G. **1960**. [The energy of earthquakes]. *Metody detal'nogo izucheniia seismichnosti [Methods of detailed study of seismicity]*. Moscow: USSR Acad. of Sci. Publ., 176: 75–114. (In Russ.).
23. Riznichenko Iu.V. **1985**. [Problems of seismology]. In.: *Izbrannye trudy [Selected works]*. Moscow: Nauka, 408 p. (In Russ.).
24. Scholz C.H. **2019**. *The mechanics of earthquakes and faulting*. 3<sup>rd</sup> ed. Cambridge: Cambridge Univ. Press, 519 p. <https://doi.org/10.1017/9781316681473>
25. Scuderi M.M., Marone C., Tinti E., Di Stefano G., Collettini C. **2016**. Precursory changes in seismic velocity for the spectrum of earthquake failure modes. *Nature Geoscience*, 9(9): 695–700. <https://doi.org/10.1038/ngeo2775>

26. Sim L.A., Marinin A.V., Sycheva N.A., Sychev V.N. **2014**. The pattern of the paleo- and present-day stresses of Northern Tien Shan. *Izvestiya. Physics of the Solid Earth*, 50(3): 378–392. <https://doi.org/10.1134/S1069351314030100>
27. Snoke J.A. **1989**. Earthquake mechanisms. In: *Encyclopedia of geophysics*. Van Nostrand Reinhold Company, 239–245. [https://doi.org/10.1007/0-387-30752-4\\_2](https://doi.org/10.1007/0-387-30752-4_2)
28. Snoke J.A. **1990**. Clyde and the gopher: a preliminary analysis of the 12 May 1990 Sakhalin Island event. *Seismological Research Letters*, 61: 161.
29. Snoke J.A. **2000**. *FOCMEC: FOCal MEChanism determinations: A manual*. URL: [www.geol.vt.edu/outreach/vtso/focmec/](http://www.geol.vt.edu/outreach/vtso/focmec/) (access date: 10.04.2020).
30. Sychev I.V., Koulakov I., Sycheva N.A., Koptev A., Medved I., Khrepy S.E., Al-Arifi N. **2018**. Collisional processes in the crust of the Northern Tien Shan inferred from velocity and attenuation tomography studies. *J. of Geophysical Research: Solid Earth*, 123(2): 1752–1769. <https://doi.org/10.1002/2017JB014826>
31. Sychev V.N., Sycheva N.A. **2018**. *Programmnyi kompleks CodaQ rascheta dobrotnosti sredy na osnove modeli odnokratnogo rasseianiia [The CodaQ software complex for the Q-factor calculating on the base of single scattering model]*: [authorship certificate 2018610919 (KG); Research Station RAS in Bishkek city. no. 2017614787]; application 25.05.2017; publ. 19.01.2018. (In Russ.).
32. Sychev V.N., Sycheva N.A., Imashev S.A. **2019**. Study of aftershock sequence of Suusamyr earthquake. *Geosistemy perekhodnykh zon = Geosystems of Transition Zones*, 3(1): 35–43. (In Russ.). [doi.org/10.30730/2541-8912.2019.3.1.035-043](https://doi.org/10.30730/2541-8912.2019.3.1.035-043)
33. Sycheva N.A., Bogomolov L.M. **2014**. Stress drop in the sources of intermediate-magnitude earthquakes in Northern Tien Shan. *Izvestiya, Physics of the Solid Earth*, vol. 50 (3): 415–426. <https://doi.org/10.1134/s1069351314030112>
34. Sycheva N.A., Bogomolov L.M. **2016**. Patterns of stress drop in earthquakes of the Northern Tien Shan. *Russian Geology and Geophysics*, 57(11): 1635–1645. <https://doi.org/10.1016/j.rgg.2016.10.009>
35. Sycheva N.A., Mansurov A.N. **2017**. Comparison of crustal deformation rates estimated from seismic and GPS data on the Bishkek Geodynamic Polygon. *Geodinamika i tektonofizika = Geodynamics & Tectonophysics*, 8(4): 809–825. <https://doi.org/10.5800/gt-2017-8-4-0318>
36. Reasenbergh P.A., Oppenheimer D. **1985**. FPFIT, FPLOT and FPPAGE: FORTRAN Computer Programs for Calculating and Displaying Earthquake Fault-Plane Solutions. *US Geological Survey Open-File Report*, 85–739. 109 p.
37. Roecker S.W., Sabitova T.M., Vinnik L.P., Burmakov Y.A., Golvanov M.I., Mamatkanova R., Munirova L. **1993**. Three-dimensional elastic wave velocity structure of the Western and Central Tien Shan. *J. of Geophysical Research*, 98(B9): 15779–15795. <https://doi.org/10.1029/93jb01560>
38. Ruff L.J. **1999**. Dynamic stress drop of recent earthquakes: Variations within subduction zones. *Pure and Applied Geophysics*, 154: 409–431. <https://doi.org/10.1007/s000240050237>
39. Tsallis C. **1988**. Possible generalization of Boltzmann-Gibbs statistics. *J. of Statistical Physics*, 52(1–2): 479–487. <https://doi.org/10.1007/bf01016429>
40. Yagi Yu. **2004**. *Determination of focal mechanism by moment tensor inversion*. Tsukuba: ISEE Lecture Note, 51 p.
41. Yunga S.L. **1990**. [Methods and results of study of seismotectonic deformations]. Moscow: Nauka, 191 p. (In Russ.).
42. *Zemnaia kora i verkhniaia mantiia Tian'-Shania v sviazi s geodinamikoi i seismichnost'iu [The Earth crust and upper mantle of the Tien Shan in connection with geodynamics and seismicity]*. **2006**. Ed. A.B. Bakirov. Bishkek: Ilim, 116 p. (In Russ.).

### About the Author

SYCHEVA Nailia Abdullova (ORCID 0000-0003-0386-3752), Cand. Sci. (Phys. and Math.), Senior Researcher, the GPS laboratory, Research Station of the RAS in Bishkek city, Kyrgyzstan, [nelya@gdir.ru](mailto:nelya@gdir.ru)